Dual-Parameter Fiber Sensors for Salinity and Temperature Measurement Based on a Tapered PMF Incorporated With an FBG in Sagnac Loop

Yuhui Liu, Weihao Lin, Fang Zhao, Xuming Zhang, *Member, IEEE*, and Li-Yang Shao, *Senior Member, IEEE*

***Abstract*—A flexible and stable optical fiber sensor based on the Sagnac loop is proposed and experimentally demonstrated for the measurement of salinity and temperature, simultaneously. The sensing unit consists of a tapered polarization maintaining fiber (tPMF) and a fiber Bragg grating (FBG) connected in series in the Sagnac loop. The temperature response comes from the high birefringence of PMF inside Sagnac loop, and the salinity response is enabled by the high-order modes excited in the tapered area of PMF. Besides, the FBG is for temperature compensation. We have succeeded in implementing dual-parameter measurements with the sensitivities of 0.356 nm/‰ for salinity and 0.616 nm/°C for temperature, respectively. The designed sensor has the potential for long-term monitoring of real ocean states.**

***Index Terms*—Dual-parameter sensors, Sagnac loop, salinity sensors, temperature sensors, tPMF.**

I. Introduction

OCCUPIES vast majority of the planet, the ocean is home to a large amount of species and has inexhaustible resources, making it vital to the destiny of all humankind. Technology is developing rapidly nowadays, as a result the ocean is constantly being exploited to promote sustainable economic development. However, complex marine environment seriously restricts the actual exploration rate, and exploration inevitably has an impact on the ocean and marine ecology at the same time [1], [2]. Marine environment parameters such as salinity, temperature and pressure are indispensable for long-term stable monitoring. The measured data not only provides feedback on the state of the oceans and marine environmental assessments but also serves as the basis for further exploitation activities of the ocean, thus participating in the planning of sustainable coastal economic development [3], [4], [5]. As industrialized wastewater is discharged into the ocean, the physical and chemical parameters of seawater change somewhat, starting with the refractive index (RI). Therefore, to monitor changes in the ocean, tools that can directly and precisely measure its RI are required.

With particularly favorable gifts of nature, optical fiber has outstanding performance in the field of sensors in addition to communication [6], [7]. The low cost allows large number of preparations and wide range of applications, the small size and light weight make it easy to transport and lay to suit various scenarios, and more importantly, the anti-electromagnetic interference performance, can obtain more accurate sensing results. Since the working environment is in the ocean, corrosion and high-pressure resistance are also prominent advantages. Optical fiber sensing can be well adapted and applied to the salinity [8], temperature [9], [10], [11], and depth [12], [13] measurement of the ocean, which is a powerful tool for ocean exploration. A polymer-covered Mach–Zehnder interferometer (MZI) applying both arc-shaped and misaligned structures was proposed with a temperature response of 0.953 nm/°C [14]. However, due to the strong randomness of the operation process, the reproducibility of the scheme is poor, and because the presence of UV glue, it is impossible to support measurements in harsh conditions. The hydrofluoric acid (HF) etched cavity was used to form the Fabry–Perot cavity (FP), and the Vernier effect was utilized to achieve salinity measurement with a sensitivity of 6830.0 nm/RIU [15]. HF is a well-known highly corrosive chemical. Even gel-like HF employed in this preparation might pose a hazard. Even ignoring the complexity and difficulty of the operation, the high sensitivity of these works is basically oriented to a single parameter, and it is impossible to measure multiple parameters at the same time. Compared to common MZI and FP structures, Sagnac loop structure is easier to construct, more repeatable, and more stable. Thanks to its own advantages, two beams of light propagate simultaneously in the clockwise and counterclockwise directions in the Sagnac loop and form interference [16]. When simple fiber structure adjustment or modification is supplemented on

Manuscript received 29 December 2023; accepted 4 January 2024. Date of publication 9 January 2024; date of current version 30 January 2024. This work was supported in part by the Department of Natural Resources of Guangdong Province, under Grant GDNRC [2022] No. 22, in part by the Science, Technology and Innovation Commission of Shenzhen Municipality under Grant 20220815121807001, in part by the Intelligent Laser Basic Research Laboratory under Grant PCL2021A14-B1, in part by the Research Grants Council (RGC) of Hong Kong under Grants 15215620, N_PolyU511/20, and PDFS2021-2S02, and in part by The Hong Kong Polytechnic University under Grants 1-CD4V, G-SB4J, 1-YY5V, 1-CD6U, 1-BBEN, and 1-W28S. *(Corresponding authors: Xuming Zhang; Li-Yang Shao.)*

Yuhui Liu, Weihao Lin, and Fang Zhao are with the Department of Electrical and Electronic Engineering, Southern University of Science and Technology, Shenzhen 518005, China (e-mail: 12068026@mail.sustech.edu.cn; 11510630@mail.sustech.edu.cn; 12031197@mail.sustech.edu.cn).

Xuming Zhang is with the Department of Applied Physics, Hong Kong Polytechnic University, Hong Kong SAR 999077, China (e-mail: apzhang@polyu.edu.hk).

Li-Yang Shao is with the Department of Electrical and Electronic Engineering, Southern University of Science and Technology, Shenzhen 518005, China, and also with the Peng Cheng Laboratory, Shenzhen 518005, China (e-mail: shaoly@sustech.edu.cn).

Digital Object Identifier 10.1109/JPHOT.2024.3351092

its initial form, it can achieve performance superior to the above structures. Apart from that, the Sagnac loop sensing module is more like a stand-alone unit, which can be simply associated with light source and spectrometer by a coupler or a circulator. The benefit is that it can be easily connected to the end of a long conductor to enable far away distance monitoring, which is necessary for actual ocean monitoring [17]. By applying tapered side hole fiber (SHF) in Sagnac loop, a dual-parameter sensor achieving sensitivity of 0.2867 nm/‰ for salinity measurement and 0.3041 nm/°C for temperature measurement was presented [18]. Nonetheless, there is a problem that the cross-sensitivity phenomenon makes it impossible to measure the two parameters simultaneously.

Since temperature directly affects the density of the liquid, it leads to a variation in the RI. Cross-sensitive makes it impossible to accurately analyze the reading results of the fiber optic sensor when the temperature and salinity varies in same period. In the process of measuring the RI, the monitoring results can be obtained more accurately when avoiding the influence of temperature changes. However, this will be more demanding on the monitoring conditions. A cascade sensor of FP and MZI was proposed to solve the problem of cross-sensitivity of salinity and temperature, which used a laser to etch a U-shaped defect [19]. Even if high sensitivity was obtained, the mechanical strength of the structure was sacrificed, and the manufacturing difficulty and cost were greatly increased, making it difficult to be widely used. Cascading FBG is an effective way to solve temperature-induced crosstalk in many studies [20], [21]. FBG has same spacing gratings on single mode fiber formed by periodically laser etching. It has a specific spectrum and is only temperature modulated, although the modulation shift is small. By welding FBG to a multimode fiber with micro bubbles, temperature and pressure monitoring were realized simultaneously, and performance tests were carried out in cardiovascular simulations. It is expected to be applied to minimally invasive surgery [22]. A polyimide coated FBG was also designed to meet the demand of measuring salinity and temperature simultaneously [23]. Still, the use of organic materials, structural complexity, low repeatability, and low temperature sensitivity limit their application in marine monitoring. Therefore, salinity and temperature marine sensors with simple fabrication, high repeatability, low cost, and high responsivity are urgently needed to be presented.

In this article, a fiber sensor for simultaneous detection of salinity and temperature is proposed. An FBG and a tPMF, with a waist of 6.8 μm, connect in series in the Sagnac loop to form the sensing unit. The sensor with the sensitivity of 0.356 nm/‰ for salinity measurement is achieved. At the same time, the sensor has the response to temperature, and with the help of high birefringence index of PMF [24], the temperature measuring can reach sensitivity of 0.616 nm/°C in the range of 22 °C–36 °C. Thanks to the temperature compensation provided by FBG, dual-parameter measurement of salinity and temperature can be realized. The designed system for simultaneous monitoring of dual parameters has strengths of simple structure, low hardware requirements, low cost, and easy preparation, which has been verified in laboratory level for the monitoring of salinity and temperature. It is expected to be applied to practical ocean monitoring.

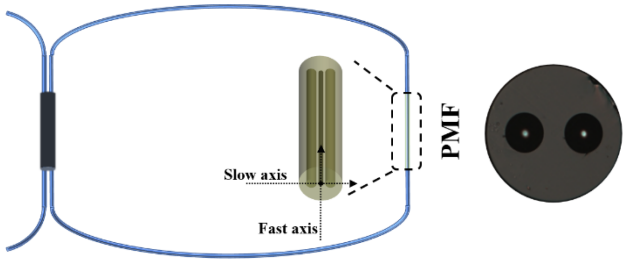

Fig. 1. Schematic diagram of PMF in Sagnac loop.

II. Experimental Principle and Setup

A. Principle of PMF in Sagnac Loop

Fig. 1 describes the basic working principle of PMF in Sagnac loop. In the beginning, light from broadband source (BBS) enters the Sagnac loop through a 3 dB coupler, transmits in both clockwise and counterclockwise directions, creating a phase difference ϕ. Two beams of light meet again and interfere with each other at the coupler. The final signal then outputs to the optical spectrum analyzer (OSA). At initial condition of Sagnac loop, the output light intensity I_{out} has a relationship with the input I_{in}, that is $I_{\text{out}} = t \cdot I_{\text{in}}$. t represents the transmittance and can be expressed as the following equation:

$$t = \frac{1 - \cos\phi}{2} \tag{1}$$

Barely, SMF leads tiny phase changes and requires a long length to achieve Sagnac effect. The utilization of highly birefringence fibers like PMF, which has difference RIs as n^o_{eff} for ordinary wave in fast axis and n^e_{eff} for extraordinary wave in slow axis, can greatly shorten the length of the fiber used and significantly expand phase differentiation ϕ, which can be given as:

$$\phi = 2\pi \frac{BL}{\lambda} \tag{2}$$

in which, $B = n^o_{eff} - n^e_{eff}$ refers to the birefringence of PMF, while L represents the length of the PMF spliced and fused into the loop. λ is the wavelength of light. Due to the extremely high birefringence characteristic, a section of PMF introduced into the loop, not only helps to realize the Sagnac effect, but also greatly improves the sensing response to temperature. At the resonance dip of the transmission interference spectrum, the condition of $\phi = (2k+1)\pi$ is satisfied, i.e., $\lambda_{dip} = 2BL/(2k+1)$, where k is an integer. When the surrounding temperature T changes, the temperature sensitivity S_T of this sensor can be expressed as [25]:

$$S_T = \frac{\Delta_{\text{output}}}{\Delta_{\text{input}}} = \frac{\Delta\lambda}{\Delta T} = \frac{dB}{dT}\frac{\lambda}{B} + \frac{dL}{dT}\frac{\lambda}{L} \tag{3}$$

The effect of temperature on the SMF quartz material is minimal, and the PMF's length variation amounts come from

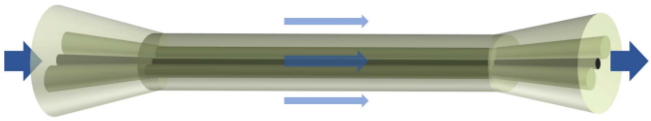

Fig. 2. Schematic diagram of tPMF.

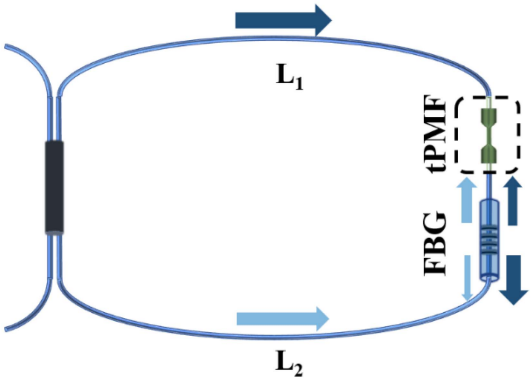

Fig. 3. Schematic diagram of FBG in Sagnac loop.

temperature is negligible comparing to its total length. Therefore, the temperature response mainly results from the B of PMF.

B. Principle of tPMF

Since the Sagnac structure and PMF itself are not sensitive to the RI, the response to salinity can be further introduced by tapering PMF to tPMF. As shown in Fig. 2, when passing through the tapered area, a part of light leaks into the surroundings around the fiber waist. The RI difference between the environmental and the fiber causes the optical path difference, and the light entering the fiber again interferes with the light in the original optical path. At this time, the sensor can response to RI, the phase differentiation φ bought by tPMF can be written as:

$$\varphi = 2\pi \frac{\Delta n_{eff}}{\lambda} l \tag{4}$$

where, Δn_{eff} is the RI difference between tPMF core mode and effective index of cladding mode. l represents the effective length of interferometer. The dip wavelength can be given as $\lambda_{dip} = 2\Delta n_{eff} l/(2m+1)$, l is fixed, and m is an integer [26]. Therefore, the RI sensitivity S_{RI} can be expressed to [27]:

$$S_{RI} = \frac{\Delta\lambda}{\Delta n} = \frac{d\Delta n_{eff}}{dn} \frac{\lambda}{\Delta n_{eff}} \tag{5}$$

Through tapering operation, the salinity variation can be measured. However, the light leaking at this structure inevitably makes the sensing system suffer from large transmission loss, which is about 18 dBm.

C. Principle of FBG in Sagnac Loop

FBG structure is shown in Fig. 3. It is able to work as a sensor with periodic changes in the RI of optical fiber. When the light propagates in FBG, most of light pass through the gratings, while light waves of specific wavelength is reflected due to different refractive properties. The Bragg wavelength λ_B can be expressed as [28]:

$$\lambda_B = 2n\Lambda \tag{6}$$

wherein, n is effective RI of fiber core, Λ refers to interval length between gratings. Temperature effects both the n and Λ, and the warmth sensitivity of FBG can be calculated as:

$$S_T = \frac{\Delta\lambda_B}{\Delta T} = (\alpha_n + \alpha_\Lambda)\ \lambda_B \tag{7}$$

here, wavelength movement is expressed by $\Delta\lambda_B$, α_n and α_Λ represent thermo-optical and thermo-expansion coefficient, respectively.

When FBG is connected in series into the Sagnac loop as shown in Fig. 3, the clockwise (dark blue) and counterclockwise (light blue) light passing through the FBG has the same optical path, that equals to $L_1 + L_2$, which is equivalent to the basic SMF Sagnac loop structure and has no effect on the spectrum. As L_1 has different value with L_2, interference occurs when the reflected waves meet at the coupler because two beams of reflected light passing through different optical paths. Furthermore, due to the presence of tPMF in one side in this experiment, there must be path difference of the light reflected by FBG in two directions. These parts of light then interfere at the 3 dB coupler [29].

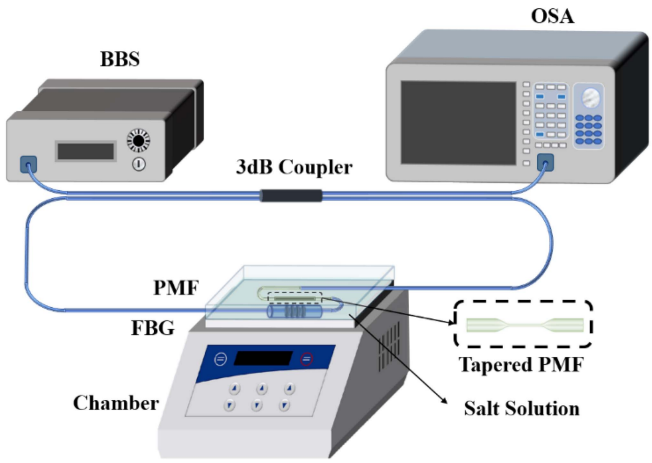

Fig. 4. Schematic diagram of dual-parameter measurement setup under BBS.

D. Setup of tPMF and FBG in Sagnac Loop

The entire experiment was conducted under the condition of using a BBS (HOYATEK, HY-SLED-1550-10-90-8-FC/APC-T) as the light input. Illustrated in Fig. 4, broad-spectrum light enters the ring part by 3 dB coupler. Light passes in two directions through tPMF and FBG, respectively, and finally meets at the coupler and outputs to the OSA. Where the length of PMF chosen for this experiment is 30 cm, it is tapered by the tapering machine (AFBT-8000LE-H0, Shandong Coupler Technology Co., Ltd., Jinan, Shandong, China) under the parameter of 15000

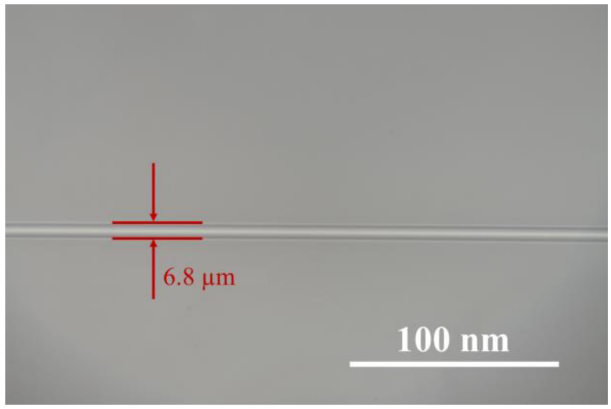

Fig. 5. Waist diameter of tapered PMF.

pulling length. As shown in Fig. 5, the waist of tPMF is about 6.8 μm. The working principle of the tapering machine is to heat and then pull the fiber at two sides. Generally, longer pulling length results in thinner fiber waist. While using thinner fiber in the sensing system, better performance in sensing sensitivity can be reached. Unfortunately, thinner waist reduces the fiber mechanical strength, enlarges the transmission loss and lows repeatability. Here, after taking sensitivity, transmission loss, and fabrication repeatability into account, the parameters chosen in the experiment result in a fairly balanced sensor performance in these aspects. FBG utilized in this experiment has a center wavelength of 1544.906 nm with bandwidth of 0.227 nm. Its side mode rejection ratio is 16 dB. And its grating length is 10 mm. The tPMF and FBG sharing the role of sensing are fixed together on the temperature control platform (MK-20, Allsheng, Hangzhou, China). The commercial temperature chamber is warmth adjustable and has a precision of 0.1 °C. During the whole test, both tPMF and FBG are completely soaked by the specified solutions to simulate actual ocean tests.

III. Result

The salinity test is finished under temperature of 25 °C. The instrumentation and the prepared simulated seawater samples were kept at a room temperature of approximately 25 °C. 25 °C is a temperature at which the sensing system can reach a steady state more quickly and it is also a reasonable value in the seawater temperature range. As shown in Fig. 6, the wavelength dip is jointly decided by both Sagnac loop and tPMF, while the peak of FBG stays stable at about 1545 nm and has no influence with interference spectra, which can be seen obviously in Fig. 7 and dark blue dots in Fig. 8. As for interference spectra, when salinity grows, the spectrum has a red shift. The linear fitting shows good linearity on salinity sensing with R square more than 0.998 and the salinity measurement sensitivity is 0.356 nm/‰ within range from 0‰ to 40‰.

When measuring the temperature variation, the environment salinity around the sensing unit is 40‰ and kept no change. In order to make the test results more consistent with the realistic situation, a common seawater concentration of 40‰

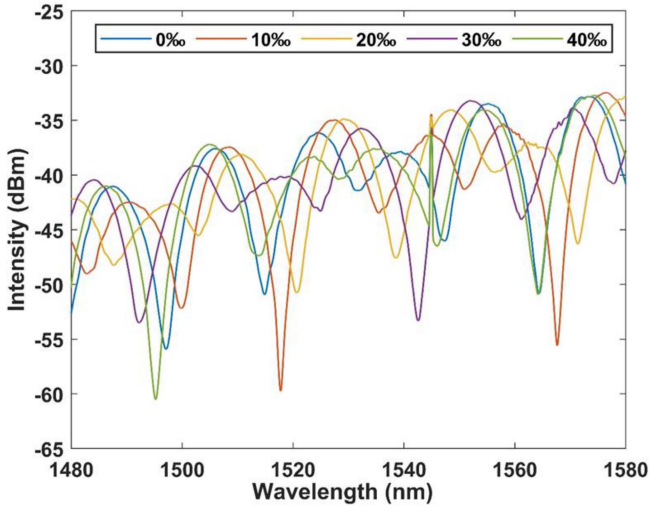

Fig. 6. Spectrum of sensing system under different salinity.

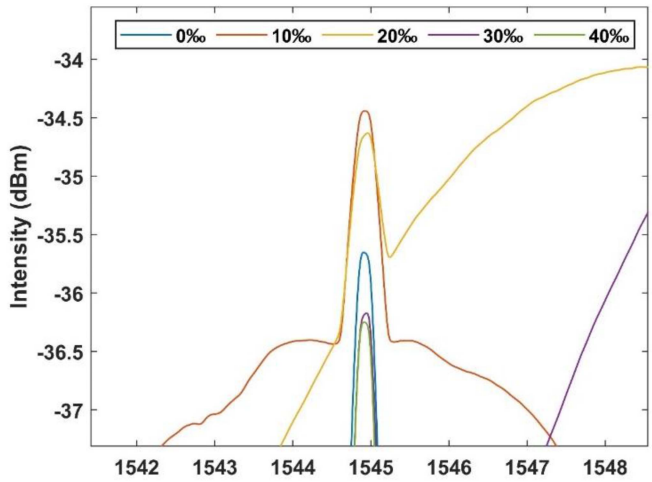

Fig. 7. FBG spectrum of the system under different salinity.

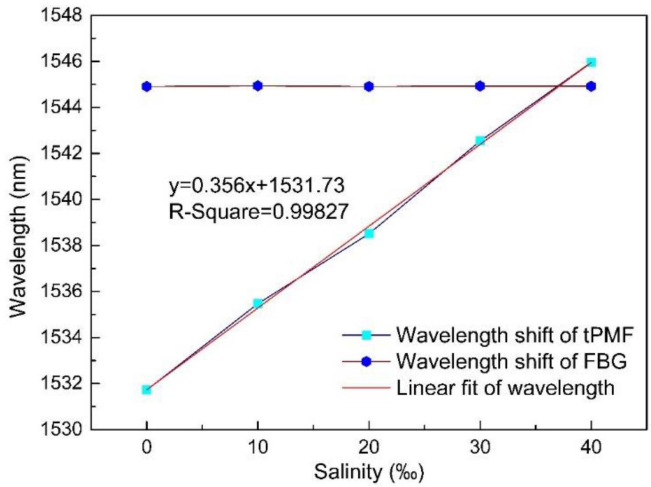

Fig. 8. Linear fitting curve for salinity sensing.

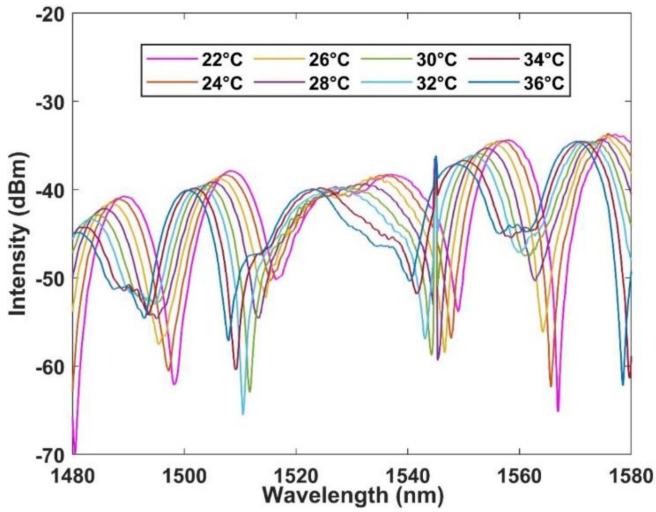

Fig. 9. Spectrum of sensing system under different warmth.

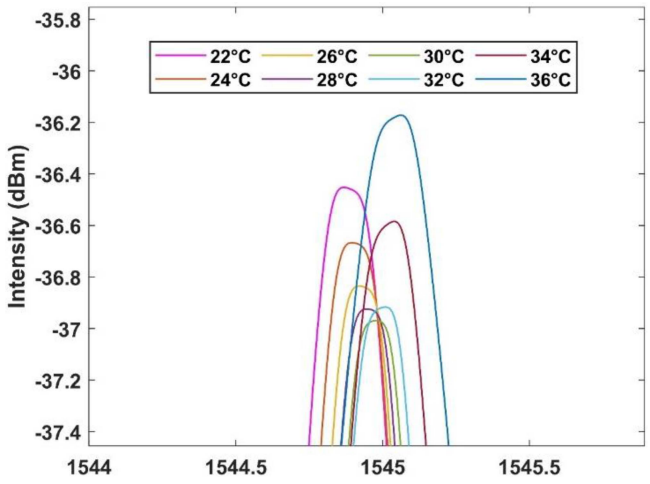

Fig. 10. FBG spectrum of the system under different warmth.

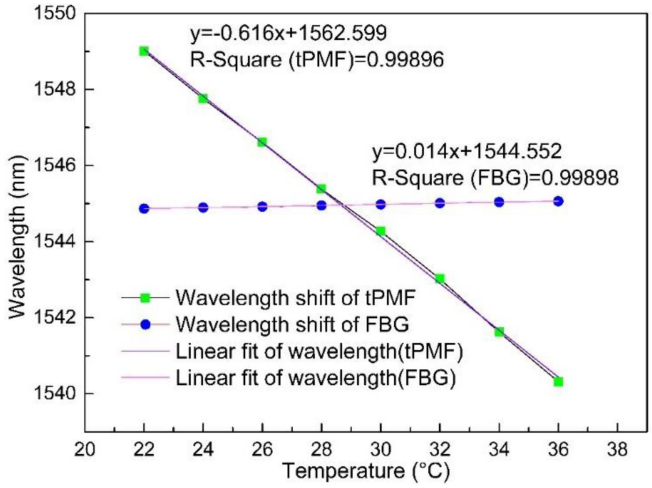

Fig. 11. Linear fitting curve for temperature sensing.

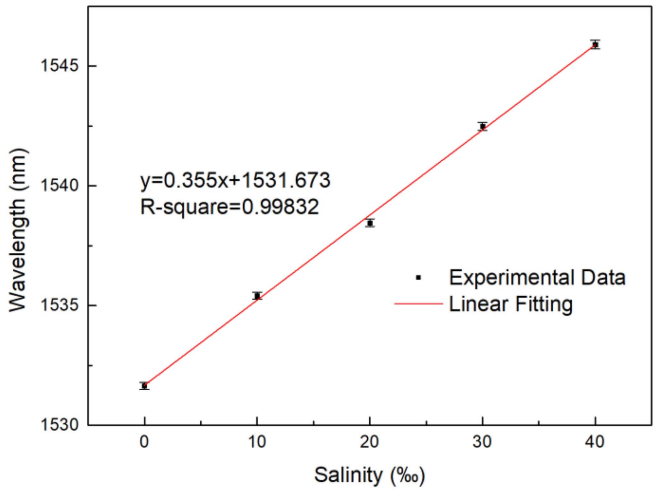

Fig. 12. Linear fitting curve for salinity sensing with matrix calibration.

was selected. From the Fig. 9, there is a blue-shift of interfence spectrum as temperature increases. While the spectrum of FBG has a opposite movement due to the different response principle, as illustrated in Fig. 10. The modulations of the spectrum by the two parts do not interfere with each other. After analyzing the data in Fig. 11, both the responses of FBG and tPMF in Sagnac loop exhibites good linearity. The temperature sensitivity of FBG is 0.014 nm/°C, and which of tPMF in ring is -0.616 nm/°C, both with high R^2 more than 0.998.

Furthermore, in order to simultaneously obtain salinity and temperature monitoring results from single measurement data, the matrix methodology, a way for dealing with simultaneous variation of double parameters, is applied. When the two sensing units in the system are sensitive to the two measured parameters at the same time, and have a linear relationship with different sensitivity coefficients, two independent equations can be formed, respectively. The change in the two parameters can then be determined by solving the system of equations. In this experiment, since the FBG only response to the warmth, the accurate temperature can be directly read by the wavelength movement of FBG spectrum. The temperature result is then substituted in the acquired interference spectrum to get the answer of salinity. The relationship can be expressed in a matrix approach as follow [20]:

$$\begin{pmatrix} \Delta\lambda_{tPMF} \\ \Delta\lambda_{FBG} \end{pmatrix} = \begin{pmatrix} 0.356 & -0.616 \\ 0 & 0.014 \end{pmatrix} \begin{pmatrix} \Delta SALINITY \\ \Delta T \end{pmatrix} \quad (8)$$

Based on actual multiple measurements, from our calculations, under temperature changes, the standard error of matrix demodulation is 0.163 nm compared to the stable temperature situation, as shown in Fig. 12. Besides, the sensitivity of the sensor is 0.355 nm/‰ which is equivalent to the result as shown in Fig. 8. The result shows both the consistency and repeatability for our designed sensing system.

The dual-parameter detection of salinity and temperature can be carried out with the temperature compensation of FBG.

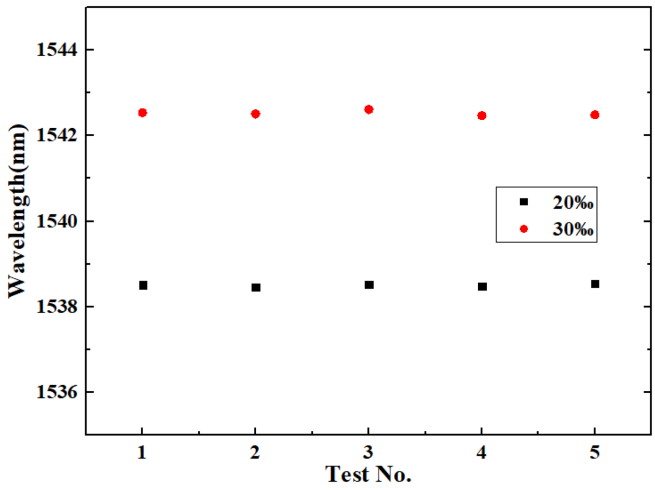

Fig. 13. Stability test for salinity sensing.

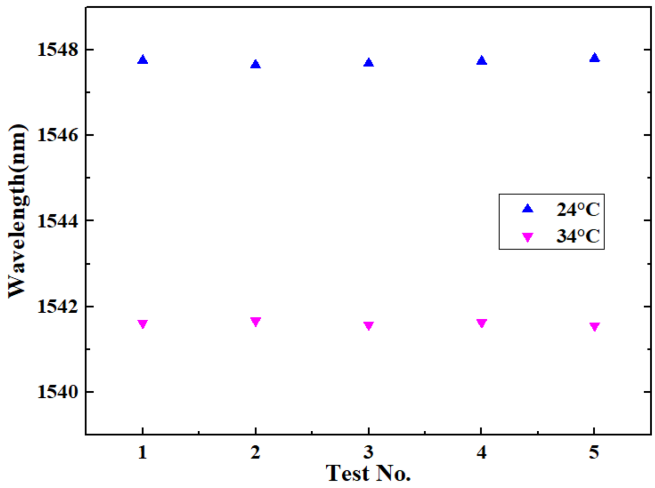

Fig. 14. Stability test for temperature sensing.

TABLE I
COMPARISON BETWEEN THE PROPOSED SENSOR AND REFERENCES

Ref	Structure	S_T (nm/°C)	$S_{SALINITY}$ (nm/‰)
[30]	U-shaped tapered fiber	0.115	0.068
[31]	U-shaped few-mode fiber	~	0.185
[32]	SPR-MZI	0.317	0.429
[33]	Semi-Open Cavity	1.280	0.309
[34]	balloon shaped SMF	0.735	0.168
This work	tPMF- Sagnac loop	0.616	0.356

Table I shows the cmparision betweent different kind of dual-parameter fiber sensors, the result proves that the sensing unit has excellent performance.

Futhermore, the stability measurements for salinity and temperature sensing were also tested for five times each, as shown in Figs. 13 and 14. The difference in salinity test is less than 0.14 nm, and that in temperature measurement is less than 0.16 nm. The data difference is very small, which reflects the good repeatability on salinity and temperature measurements of the sensing system. High resolution and stability ensure the application of realistic ocean measurements. Besides, due to the cumbersomeness of usual OSA in lab, portable OSAs provide choices for practical test. Additionally, using a spectrum interrogator to demodulate the intensity is also another effective approach.

IV. CONCLUSION

In conclusion, a dual-parameter fiber sensor for the measurement of salinity and temperature are realized by serial connection of tPMF and FBG inside the Sagnac loop. Thanks to the high birefringence of PMF, the temperature monitoring has achieved the sensitivity of 0.616 nm/°C. And the chose of a tPMF with a waist of 6.8 μm enhances the reaction between the environment salinity change and fiber core, and has yielded a sensitivity of 0.356 nm/‰. The FBG facilitates temperature compensation and eliminates the errors caused by cross-sensitivity problem. The designed fiber sensing structure enables to accurate measure the salinity of seawater under temperature interference, which is conducive to practical marine applications and has great application prospects.

REFERENCES

[1] F. Chai et al., "Monitoring ocean biogeochemistry with autonomous platforms," *Nature Rev. Earth Environ.*, vol. 1, no. 6, pp. 315–326, Jun. 2020, doi: 10.1038/s43017-020-0053-y.
[2] R. Min, Z. Liu, L. Pereira, C. Yang, Q. Sui, and C. Marques, "Optical fiber sensing for marine environment and marine structural health monitoring: A review," *Opt. Laser Technol.*, vol. 140, 2021, Art. no. 107082, doi: 10.1016/j.optlastec.2021.107082.
[3] Z. Liu, S. Zhang, C. Yang, W.-H. Chung, and Z. Li, "Submarine optical fiber sensing system for the real-time monitoring of depth, vibration, and temperature," *Front. Mar. Sci.*, vol. 9, 2022, Art. no. 922669, doi: 10.3389/fmars.2022.922669.
[4] S. Chen et al., "Marine structural health monitoring with optical fiber sensors: A review," *Sensors*, vol. 23, no. 4, 2023, Art. no. 1877, doi: 10.3390/s23041877.
[5] C. R. U. Kumari, D. Samiappan, R. K., and T. Sudhakar, "Fiber optic sensors in ocean observation: A comprehensive review," *Optik*, vol. 179, pp. 351–360, 2019, doi: 10.1016/j.ijleo.2018.10.186.
[6] M. Elsherif et al., "Optical fiber sensors: Working principle, applications, and limitations," *Adv. Photon. Res.*, vol. 3, no. 11, 2022, Art. no. 2100371, doi: 10.1002/adpr.202100371.
[7] C. Pendao and I. Silva, "Optical fiber sensors and sensing networks: Overview of the main principles and applications," *Sensors*, vol. 22, no. 19, Oct. 2022, Art. no. 7554, doi: 10.3390/s22197554.
[8] Y. Qian, Y. Zhao, Q. Wu, and Y. Yang, "Review of salinity measurement technology based on optical fiber sensor," *Sensors Actuators B: Chem.*, vol. 260, pp. 86–105, 2018, doi: 10.1016/j.snb.2017.12.077.
[9] R. K. Gangwar, S. Kumari, A. K. Pathak, S. D. Gutlapalli, and M. C. Meena, "Optical fiber based temperature sensors: A review," *Optics*, vol. 4, no. 1, pp. 171–197, 2023, doi: 10.3390/opt4010013.
[10] F. Zhang, X. Xu, J. He, B. Du, and Y. Wang, "Highly sensitive temperature sensor based on a polymer-infiltrated Mach–Zehnder interferometer created in graded index fiber," *Opt. Lett.*, vol. 44, no. 10, pp. 2466–2469, 2019, doi: 10.1364/ol.44.002466.
[11] W. Lin et al., "Temperature fiber sensor based on 1-D CNN incorporated time-stretch method for accurate detection," *IEEE Sensors J.*, vol. 23, no. 6, pp. 5773–5779, Mar. 2023, doi: 10.1109/jsen.2023.3238028.
[12] D. B. Duraibabu, G. Leen, D. Toal, T. Newe, E. Lewis, and G. Dooly, "Underwater depth and temperature sensing based on fiber optic technology for marine and fresh water applications," *Sensors*, vol. 17, no. 6, May 2017, Art. no. 1228, doi: 10.3390/s17061228.

[13] W. Lin et al., "Fiber ring cavity laser based on cascading two peanut-shape structures for liquid level measurement," *Proc. SPIE*, vol. 12478, pp. 677–683, 2022.
[14] X. Li, J. Tan, W. Li, C. Yang, Q. Tan, and G. Feng, "A high-sensitivity optical fiber temperature sensor with composite materials," *Opt. Fiber Technol.*, vol. 68, 2022, Art. no. 102821, doi: 10.1016/j.yofte.2022.102821.
[15] R. Flores, R. Janeiro, and J. Viegas, "Optical fibre fabry-perot interferometer based on inline microcavities for salinity and temperature sensing," *Sci. Rep.*, vol. 9, no. 1, Jul. 2019, Art. no. 9556, doi: 10.1038/s41598-019-45909-2.
[16] Y. Liu et al., "Integrated fiber ring laser temperature sensor based on vernier effect with lyot–sagnac interferometer," *Sensors*, vol. 23, no. 14, Jul. 2023, Art. no. 6632, doi: 10.3390/s23146632.
[17] Z. L. Rani et al., "Fiber-optic microstructure sensors: A review," *Photonic Sensors*, vol. 11, no. 2, pp. 227–261, Jun. 2021, doi: 10.1007/s13320-021-0632-7.
[18] F. Zhao et al., "Salinity and temperature dual-parameter sensor based on fiber ring laser with tapered side-hole fiber embedded in sagnac interferometer," *Sensors*, vol. 22, no. 21, 2022, Art. no. 8533, doi: 10.3390/s22218533.
[19] Y. Zhao, J. Zhao, X. Wang, Y. Peng, and X. Hu, "Femtosecond laser-inscribed fiber-optic sensor for seawater salinity and temperature measurements," *Sensors Actuators B: Chem.*, vol. 353, 2022, Art. no. 131134, doi: 10.1016/j.snb.2021.131134.
[20] Y. Liu et al., "Fabrication of dual-parameter fiber-optic sensor by cascading FBG with FPI for simultaneous measurement of temperature and gas pressure," *Opt. Commun.*, vol. 443, pp. 166–171, 2019, doi: 10.1016/j.optcom.2019.03.034.
[21] H. L. Hui Li, Q. Z. Qingchao Zhao, S. J. Shaodong Jiang, J. N. Jiasheng Ni, and C. W. Chang Wang, "FP cavity and FBG cascaded optical fiber temperature and pressure sensor," *Chin. Opt. Lett.*, vol. 17, no. 4, 2019, Art. no. 040603, doi: 10.3788/col201917.040603.
[22] T. Li et al., "Micro-bubble F-P cavity and FBG cascade structure-based pressure sensor with temperature self-compensation for minimally invasive surgery," *IEEE Trans. Biomed. Eng.*, vol. 69, no. 11, pp. 3288–3299, Nov. 2022, doi: 10.1109/TBME.2022.3166840.
[23] J.-Y. Guo et al., "Groundwater salinity sensing using PI-FBG with improved capillary coating method," *Measurement*, vol. 218, 2023, Art. no. 113223, doi: 10.1016/j.measurement.2023.113223.
[24] W. Lin, Y. Liu, Y. Liu, P. P. Shum, and M. I. Vai, "Fiber temperature sensor based on vernier effect and optical time stretching method," *Micromachines*, vol. 13, no. 12, Dec. 2022, Art. no. 2215, doi: 10.3390/mi13122215.
[25] L. P. Shao, J. H. Hu, H. L. Lu, J. Du, T. Y. Wu, and Y. P. Wang, "High-sensitivity temperature sensor based on polarization maintaining fiber sagnac loop," *Photonic Sensors*, vol. 9, no. 1, pp. 25–32, Mar. 2019, doi: 10.1007/s13320-018-0517-6.
[26] F. Zhao et al., "Highly sensitive salinity and temperature measurement based on tapered-SHF MZI fiber laser structure," *Meas. Sci. Technol.*, vol. 34, no. 6, 2023, Art. no. 064002, doi: 10.1088/1361-6501/acbe12.
[27] L.-P. Sun et al., "Ultrasensitive sensing in air based on Sagnac interferometer working at group birefringence turning point," *Opt. Exp.*, vol. 27, no. 21, pp. 29501–29509, 2019, doi: 10.1364/oe.27.029501.
[28] I. García, J. Zubia, G. Durana, G. Aldabaldetreku, M. Illarramendi, and J. Villatoro, "Optical fiber sensors for aircraft structural health monitoring," *Sensors*, vol. 15, no. 7, pp. 15494–15519, 2015, doi: 10.3390/s150715494.
[29] Y. Cao, H. Zhang, Y. Miao, Z. Ma, and B. Li, "Simultaneous measurement of temperature and refractive index based on microfiber Bragg Grating in Sagnac loop," *Opt. Fiber Technol.*, vol. 47, pp. 147–151, 2019, doi: 10.1016/j.yofte.2018.11.028.
[30] P. Li et al., "Simultaneous measurement of salinity and temperature of seawater based on U-shaped tapered no-core fiber," *Infrared Phys. Technol.*, vol. 130, 2023, Art. no. 104617, doi: 10.1016/j.infrared.2023.104617.
[31] W. Zhang, M. Wu, X. Wang, Z. Tong, M. Dong, and G. Yan, "Temperature insensitive salinity sensor with U-shaped structure based on few-mode fiber," *Opt. Fiber Technol.*, vol. 76, 2023, Art. no. 103218, doi: 10.1016/j.yofte.2022.103218.
[32] Y. Wang et al., "Optical fiber sensor based on SPR and MZI for seawater salinity and temperature measurement," *Opt. Laser Technol.*, vol. 162, 2023, Art. no. 109315, doi: 10.1016/j.optlastec.2023.109315.
[33] S. Liu et al., "Underwater temperature and salinity fiber sensor based on semi-open cavity structure of asymmetric MZI," *IEEE Sensors J.*, vol. 23, no. 16, pp. 18219–18233, Aug. 2023, doi: 10.1109/jsen.2023.3291568.
[34] T. Selokar and M. T. R. Giraldi, "All-fiber sensors for salinity and temperature simultaneous measurement," *Opt. Quantum Electron.*, vol. 53, no. 1, pp. 1–17, 2021, doi: 10.1007/s11082-020-02678-x.